CDF/ANAL/ELECTROWEAK/CDFR/6282
Version 3.0
October 29, 2004

Measurement of $W \to e\nu$ Charge Asymmetry

Cigdem Issever[a], Timothy Nelson[b], Adam Scott[a], and David Stuart[a]

[a] *University of California at Santa Barbara*
[b] *Fermilab*

Abstract

We describe a measurement of the forward-backward charge asymmetry in W production using the electron mode. The measurement provides discrimination between PDFs which is most pronounced at high $|\eta|$.

1 Introduction

Theoretical uncertainty on the parton density functions of the proton is a significant error in several measurements we will do at CDF e.g., W mass and many cross-sections. Measurement of the forward-backward charge asymmetry in $p\bar{p} \rightarrow W^{\pm}$ provides a constraint on these parton fluxes. Since u quarks carry, on average, a higher fraction of the proton momentum than d quarks, W^+ produced by $u\bar{d} \rightarrow W^+$ tend to be boosted in the proton direction. Similarly, W^- tends to be boosted in the anti-proton direction. This results in a non-zero forward-backward charge asymmetry defined as

$$A(y_W) = \frac{d\sigma(W^+)/dy - d\sigma(W^-)/dy}{d\sigma(W^+)/dy + d\sigma(W^-)/dy}\,, \tag{1}$$

where y is the rapidity of the W bosons and $d\sigma(W^{+,-})/dy$ is the differential cross section for W^+ or W^- boson production.

Leptonic decays of the W boson, in our case $W \rightarrow e\nu$, provide a cleanly identified sample for studying this asymmetry. The p_z of the neutrino is unmeasured but could be determined with a W mass constraint, up to a two-fold ambiguity. In some cases, where that ambiguity can be reduced due to the known V-A decay distribution in the W rest frame, y_W could provide a direct measure of the W production asymmetry. With sufficiently high statistics, this would likely provide the best constraint. Initially however, we use the experimentally more direct $e^{\pm}$ direction to measure the forward-backward electron asymmetry,

$$A(\eta_l) = \frac{d\sigma(e^+)/d\eta - d\sigma(e^-)/d\eta}{d\sigma(e^+)/d\eta + d\sigma(e^-)/d\eta}\,, \tag{2}$$

which convolves the W production asymmetry with the V-A decay distribution. It provides sensitivity to the ratio of the parton density functions for u and d quarks, $u(x)/d(x)$. This discrimination between pdfs is most pronounced where it is less constrained, at high values of $|\eta|$.

Thus the primary experimental challenge in this measurement is tracking in the forward region to obtain charge identification for electrons, and we begin by dicussing that. Section 2 describes the forward electron tracking algorithm. Section 3 delineates the relevant data sets, including an overview of the selection cuts. Control distributions critical to the identification of electrons and W events are shown in section 4,. Section 5 describes the W asymmetry measurement, and corrections to the asymmetry are described in sections 6 and 7. We desribe various cross-checks and systematics studies in Section 11.

2 Calorimeter–Seeded Silicon Tracking

To fully exploit the forward coverage of the silicon tracking system, we have developed a calorimeter-seeded silicon tracking algorithm, Phoenix tracking, which reconstructs the trajectories of electrons without the COT [2]. The approach is similar to the outside-in silicon tracking algorithm in which COT tracks are projected into the silicon and hits in a narrow road around the trajectory are considered for addition to the fit. The phoenix algorithm uses information from the calorimeter, rather than the COT, to seed the silicon track reconstruction. The algorithm is described in more detail in reference [2]. We briefly describe it here and focus on the charge determination performance which is critical for this analysis.

Two points and a signed curvature define a unique helix. The fitted position of the EM cluster in the shower-maximum detectors is used to determine the position of an electron candidate in the calorimeter. The position of the primary collision vertex is measured with the other tracks in the event and provides a second point for the electron trajectory. The |curvature| of the electron trajectory is determined from the transverse energy as measured by the calorimeter. These two points and the |curvature|, with appropriate covariance, are used to generate a seed helix and covariance matrix for each charge hypothesis.

These seeds are then projected into the silicon where hits are attached using the same OI pattern recognition algorithm which is used for COT-seeded tracks. Either seed can result in a silicon track if sufficient silicon hits are attached. In cases where both charge hypotheses give rise to silicon tracks, the track with the smaller χ^2/dof is chosen, where the number of degrees of freedom is simply the number of silicon hits since the helix is already fully specified by the seed track.

The Phoenix algorithm is efficient and has low background, but for this analysis we also require a low rate of charge misidentification. In the central region, the charge identification is excellent–about as good as for the COT–because the $+$ and $-$ trajectories are widely separated for electrons with $p_T \approx$ 40 GeV/c. In the plug region, however, the reduced radial lever arm between the beam and shower-maximum cluster "crowds" the $+$ and $-$ trajectories together. This makes it more difficult for the silicon pattern recognition to discriminate the charge and is particularly sensitive to the resolution of the shower-maximum position determination in the plug. To improve that resolution, we have determined alignment corrections for the PES [4] and obtain resolutions of about 1 mrad. This is sufficient to determine the charge quite robustly over the full acceptance of ISL, $|\eta| < 2$.

3 Data Sets and Selection Cuts

We select W and Z candidates from good runs between run 141544 and 168889, collected between March 2002 and September 2003. The W candidates are, of course, the signal sample. The Z candidates are used to calibrate the charge mis-identification rate.

For W candidates in the plug, we use the MET_PEM triggered data, in the bpel08 and bpel09 datasets. (The PLUG_ELECTRON trigger in those datasets is also used to measure the QCD backgrounds.) For W candidates in the central region, we use the the CENTRAL_ELECTRON_18 trigger. However, to avoid any potential charge bias from the XFT, we also use the W_NOTRACK trigger. Both triggers are in the bhel08 and bhel09 datasets. The Z candidates are from the Z_NOTRACK trigger in the bhel08 and bhel09 datasets.

Only runs passing the DQM version 4 silicon good-run criteria are selected [3] leaving about $170\,\mathrm{pb}^{-1}$ of integrated luminosity. The data are 4.8.4 production and the objects were remade in 4.10.4 with Sntntuple dev_240. We use a custom version of Phoenix tracking that incorporates our PES alignment corrections.

3.1 Electron Selection

We select electrons in two categories, COT or PHX, using baseline selection requirements plus a few additional requirements:

- Central electrons
  - $E_T > 25\,\mathrm{GeV}$
  - Iso/Em$E_T < 0.1$
  - HadE/EmE$< 0.055 + 0.00045 \times EmE$
  - Lshr< 0.2
  - Fiducial
  - CES $\chi^2 < 10$

  - A COT or PHX track.

- Plug electrons
  - $E_T > 25\,\text{GeV}$
  - HadE/EmE< 0.05
  - Iso/Em$E_T < 0.1$
  - PEM $\chi^2 < 10.$
  - PEM FitTower != 0
  - $1.2 < |\text{PES}\eta| < 2.8$
  - PES 5by9 shower profile ratio (U/V) > 0.65.
  - A PHX track.

The COT track selection requirements are:

- > 30 axial and > 30 stereo hits
- $p_T > 10$ GeV/c
- $-3 < Q \times \Delta X < 1.5$ cm
- $\Delta Z < 3$ cm
- $E/p < 2.$
- $|Z0| < 60.$ cm

The Phoenix track selection requirements are:

- $>= 4r\phi$ hits. (We ignore the r-z view).
- $\chi^2 < 8$

- $|Z0| < 60.$ cm
- $\Delta\chi^2 > 0.5$
- Seed Pull < 0.4.

The last two phoenix track selection cuts are non-standard but are aimed at rejecting cases where the charge identification is more likely to be ambiguous. If the tracking finds a track for both sign possibilities, we require that the difference between the χ^2 from the silicon hits for the two choices to be larger than 0.5. It is possible for the wrong-sign track to have a small silicon χ^2 by pulling the helix far from the seed trajectory. To discard such cases, we require that:

$$\text{Pull Ratio} \equiv \frac{\chi^2_{seed}/dof \text{ for track with lesser } \chi^2_{total}/dof}{\chi^2_{seed}/dof \text{ for track with greater } \chi^2_{total}/dof} < 0.4 \qquad (3)$$

where χ^2_{seed} is the χ^2 of the track parameters relative to the seed track.

To avoid charge bias effects, we remove plug electrons which are near noisy, disconnected, or incompletely calibrated PES strips.

3.2 $W \rightarrow e\nu$ Event Selection Cuts

In order to select a pure sample of $W \rightarrow e\nu$ events, candidates are required to have missing transverse energy $\not{E}_T > 25\,\text{GeV}$, and transverse mass in the range $50\,\text{GeV} < \text{M}_\text{T} < 100\,\text{GeV}$. To suppress QCD and Drell-Yan backgrounds, we require that there be no other EM objects with $E_T > 25\,\text{GeV}$.

3.3 $Z \rightarrow e^+e^-$ Selection Cuts

A tightly selected sample of $Z \rightarrow e^+e^-$ events is used to measure the charge mis-identification rate. When one of the electrons is tightly selected, it provides a charge tag which allows us to measure the charge mis-identification rate of the other phoenix electron. We require events with two electron candidates with $80 < M_{e^+e^-} < 100\,\mathrm{GeV}$. The tag leg is allowed up to $|\eta| = 1.5$ where the charge is easily identified. We correct for the fact that the tag charge can be wrong.

The plug energy is scaled up to set the Z mass peak appropriately. The scale factors for the east and west are consistent with each other. A scale factor of 1.078 is measured from bhel08 and 1.09 from bhel09. This energy scaling occurs in the energy used by Phoenix tracking and at the ntuple level.[1]

4 Control Distributions

To validate the W and Z selection we compare several kinematic distributions between data and Monte Carlo as shown below. We note that normalization is irrelevant here since we are not counting. Rather, we are mostly interested in checking for effects which could bias the charge determination.

Distributions from Monte Carlo and data of (e^+e^-) mass and electron E_T are compared in **Figure 1** for di-electron events. The transverse mass and E_T of $W \to e\nu$ candidates are compared to MC in **Figure 2**. The missing E_T and η are compared in **Figure 3**, and the phi distributions are compared in **Figure 4**. In all cases, the MC modelling is not excellent, but is reasonable.

[1] The energy scale used for phoenix tracking is slightly different, 1.06 and 1.09 before and after the shutdown. This is due to the fact that phoenix calculates the curvature from the total energy, EM + Hadron, of the cluster rather than just the electromagnetic component. This is a small effect at low energy but is the correct way to account for leakage in higher energy electrons.

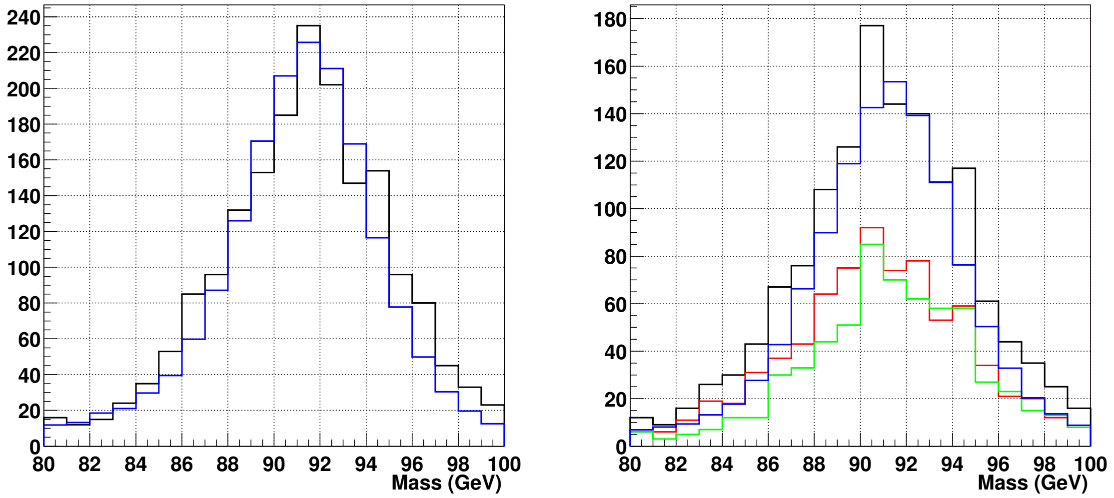

Figure 1: Dielectron mass distribution for central-central (left) and central-plug (right) events. Black is all data, blue is MC. Green is west data and red is east data.

5 W Charge Asymmetry

For the charge asymmetry measurement, $W^{\pm} \rightarrow e^{\pm}\nu$ candidates satisfying the selection cuts described in section 3 are used. The selected sample contains 49124 central and 28806 plug candidates. Phoenix tracks are used for the charge determination in all η regions, even when a COT track is also available. In the central region the W charge asymmetry measurement is performed separately using COT tracks as a cross-check.

Figure 5 shows the raw, uncorrected asymmetry as a function of η with fine and coarse η bins. To extract the true asymmetry, corrections need to be applied for effects from mis-identification of the charge and from background contributions.

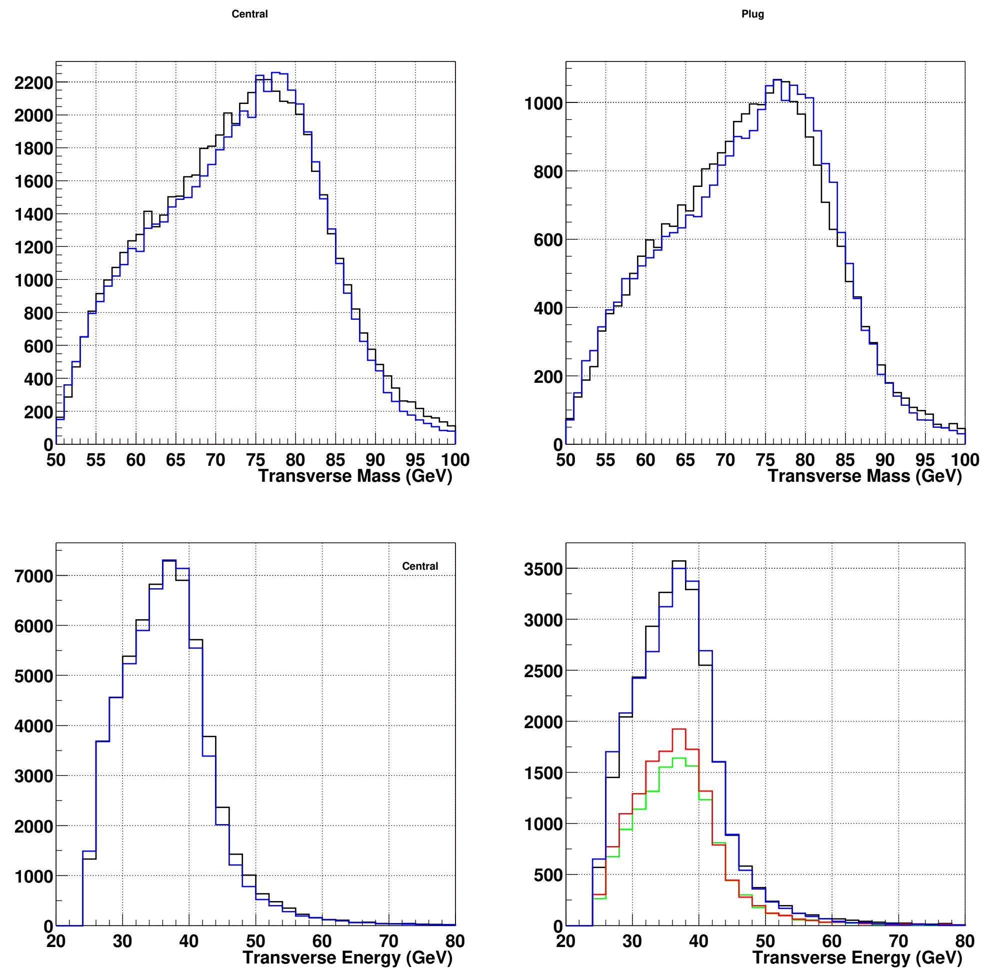

Figure 2: Top: Electron transverse mass distribution for central (left) and plug (right) events. Bottom: Electron E_T distribution for central (left) and plug (right) events. Black is data, blue is MC. Green is west data and red is east data.

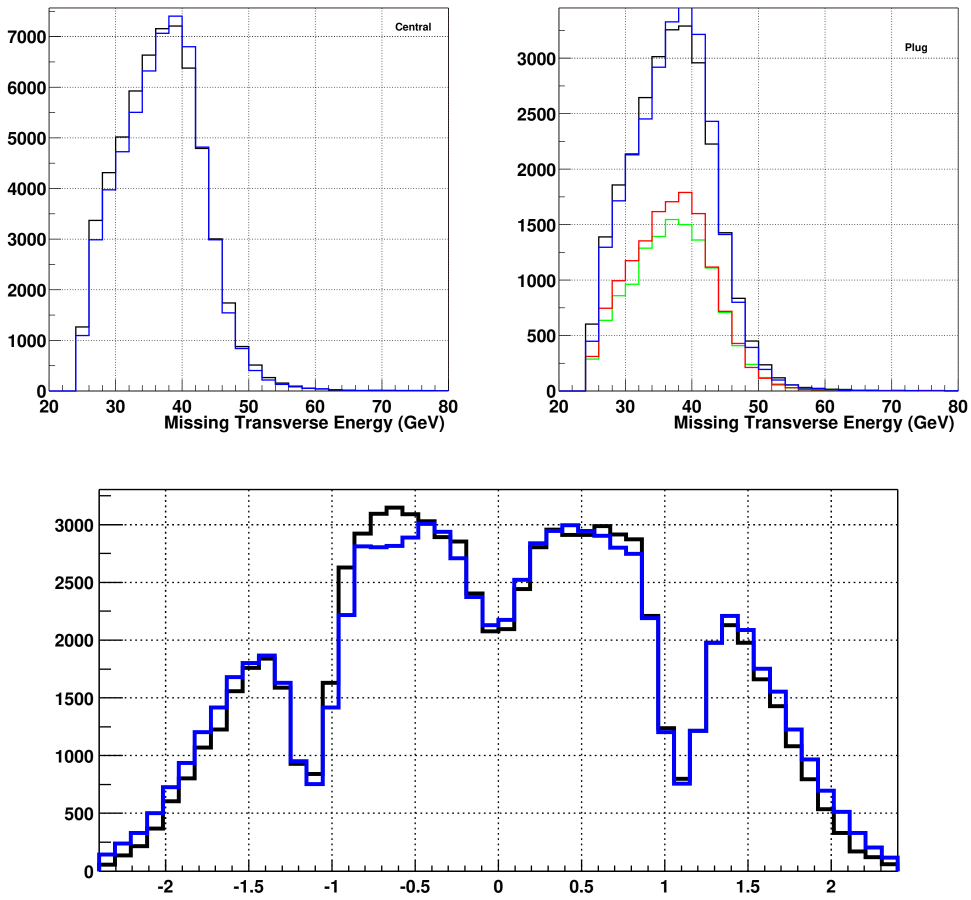

Figure 3: Top: Missing E_T distribution for central (left) and plug (right) events. (Note that the MC has no E_T cuts and the data has background apparent at low missing E_T. Bottom: Electron η distribution. Black is data, blue is MC.

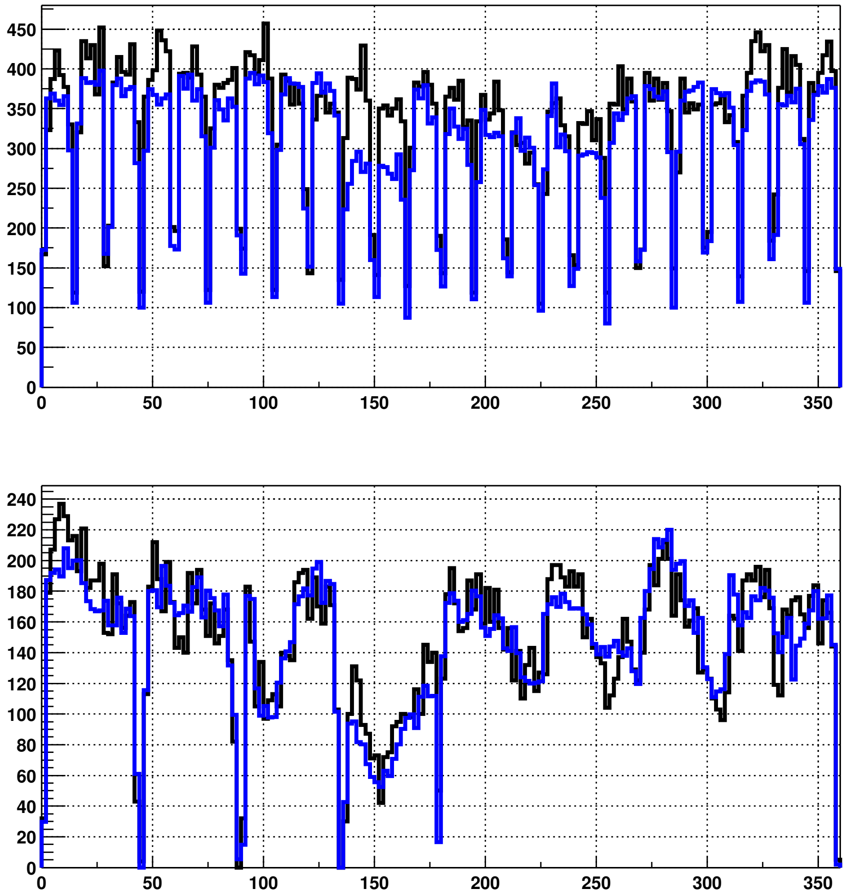

Figure 4: Phi distribution for W electron candidates from the central (top) and plug (bottom) regions. Black is data, blue is MC. The discrepancies between data and MC can be understood in terms of variations in silicon coverage. In general, the MC has too little silicon coverage because it is based on an older running configuration. Large dips in the plug arise from masking regions of the PES with dead, noisy, or miscalibrated strips.

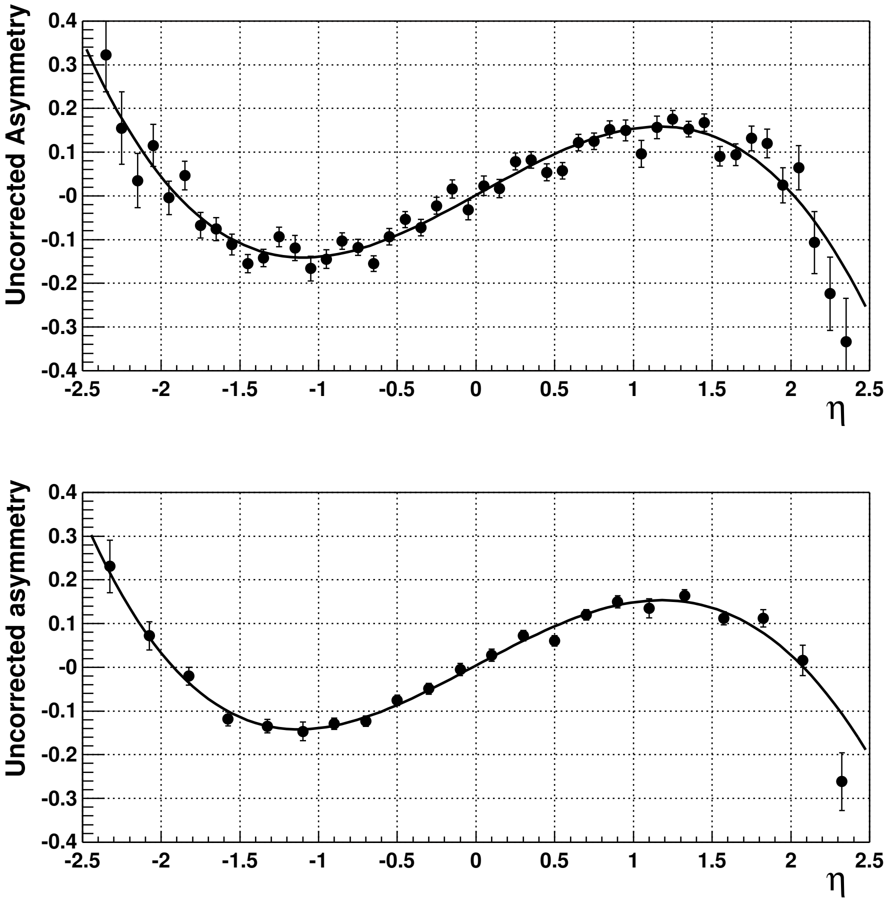

Figure 5: The raw, uncorrected, charge asymmetry is plotted as a function of η. The upper plot uses fine binning, $\Delta\eta = 0.1$, while the lower plot uses variable binning chosen for reduced uncertainty in the corrections which follow. The curves are fourth order polynomial fits drawn simply to guide the eye.

6 Charge Mis-identification

Misidentification of the charge dilutes the asymmetry, and a difference between the misidentification rate for electrons and positrons will bias the asymmetry directly. We can correct for this if we know the rate at which the charge is misidentified. Calling that misidentification rate f_+ for positrons and f_- for electrons, the true asymmetry can be computed from the measured asymmetry as

$$A = \frac{A_{\rm raw} + f_+ - f_-}{1 - f_+ - f_-}. \tag{4}$$

So, we want to make the misidentification rates small and to measure them.

Monte Carlo indicates that with the selection cuts listed above, the Phoenix algorithm provides excellent charge determination, $f \approx 1\%$, even for $|\eta| > 2$. However, the Monte Carlo is naive. Unsimulated effects such as residual misalignments in the silicon and PES would increase the charge misidentification rate in real data.

To properly account for these effects, f must be measured from the data and the uncertainty on the measured f goes directly into uncertainty on the asymmetry measurement. Since the residual misalignments may differ between the east and west plug and in fact as a function of η within each plug, f must be measured for each bin of η and the uncertainty propogated independently for each bin. This suffers from low statistics in the data, but no other approach properly incorporates the systematic uncertainties from residual misalignments, etc.

As described above, we measure $f(\eta)$ with $Z \rightarrow e^+e^-$ events where one leg provides a charge tag for the other leg. The average misidentification rate, f_Q, which does not distinguish between electrons and positrons i.e., f_+ and f_-, is shown as a function of η in **Figure 6**. The f_Q plotted in **Figure 6** takes into account the fact that the charge of the tag leg can be wrong. We measure that and correct for it, even though it is a small effect. As expected, the f_Q we measure is higher than the Monte Carlo prediction, though not much, but the uncertainty is large in the forward direction due to limited statistics.

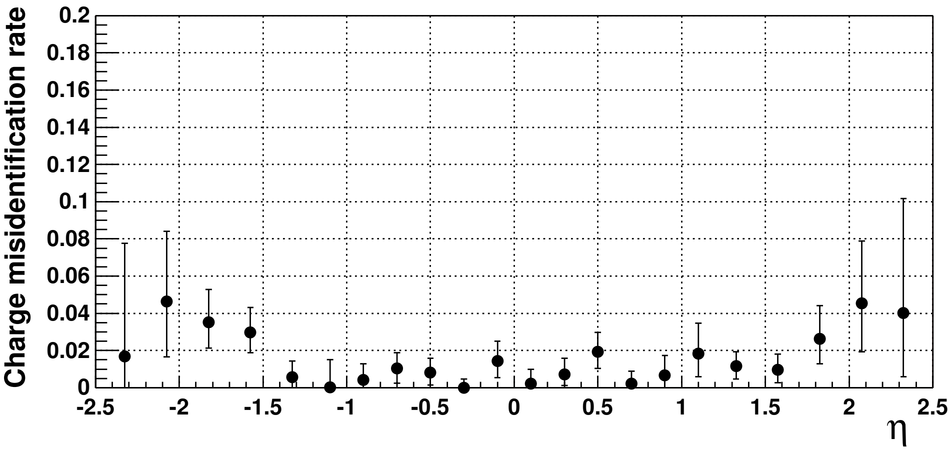

Figure 6: The charge misidentification rate, $f_Q(\eta)$, is plotted as a function of η.

The difference between the misidentification rate for positrons and electrons, $\Delta f \equiv f_+ - f_-$, is shown in **Figure 7**. The results are consistent with zero for most, but not all, bins. There is 2.5σ difference at $\eta \approx 1.8$, and the χ^2 of the points relative to zero is 37 with 22 d.o.f.

Residual misalignments are a likely source of differences between f_+ and f_- which would propagate directly into a bias on the asymmetry. We have studied the effect of misalignments by shifting the alignment constants by their uncertainty in both data and Monte Carlo. We find that such shifts cause changes in Δf and the asymmetry comparable to their uncertainties, particularly for $|\eta| > 1.5$. From this we conclude that we have no reliable measure of Δf other than that obtained directly from the data. So, we

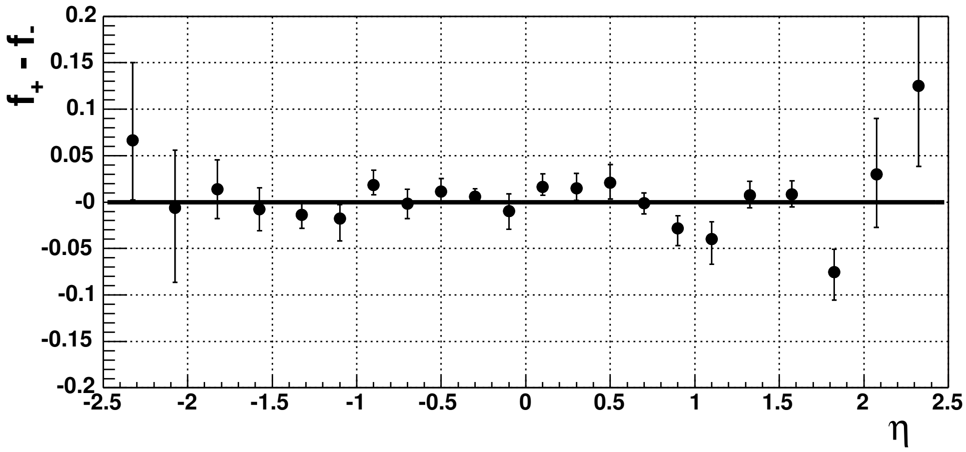

Figure 7: The difference in charge misidentification rate of positrons and electrons, $\Delta f \equiv f_+(\eta) - f_-(\eta)$, is plotted as a function of η.

use that measure to apply a correction for Δf and the uncertainty on that correction is propagated into the uncertainty on the asymmetry.

The uncertainties on $f^\pm$ are inherently asymmetric due to the combination of Poisson and binomial statistics. As advised by the Statistics Committee [5], when calculating Δf and the corrected asymmetry, we propagate these asymmetric uncertainties using a likelihood based technique described in reference [6].

7 Background Corrections

We apply corrections for three backgrounds; QCD, $Z \to e^+e^-$, and $W \to \tau\nu \to e\nu$.

Measurement of the QCD background contribution is described in CDF Note 6412 [7]. We use the standard Iso-vs-MET approach. However, to avoid correlations between isolation and other electron ID variables, most notably PEM 3x3 χ^2, we do not apply all the selection requirements in determining the QCD background. This results in an upper limit, measured to be about a factor of 2, on the background. We apply a correction to the asymmetry using as a central value half the QCD estimate and errors that are 50% of the correction. This correction is applied bin by bin in η by scaling the measured asymmetry by $1+F_{\mathrm{QCD}}/2$ where F_{QCD} is the fractional QCD estimate in that bin. The measured F_{QCD} values are shown as a function of η in **Figure 8**.

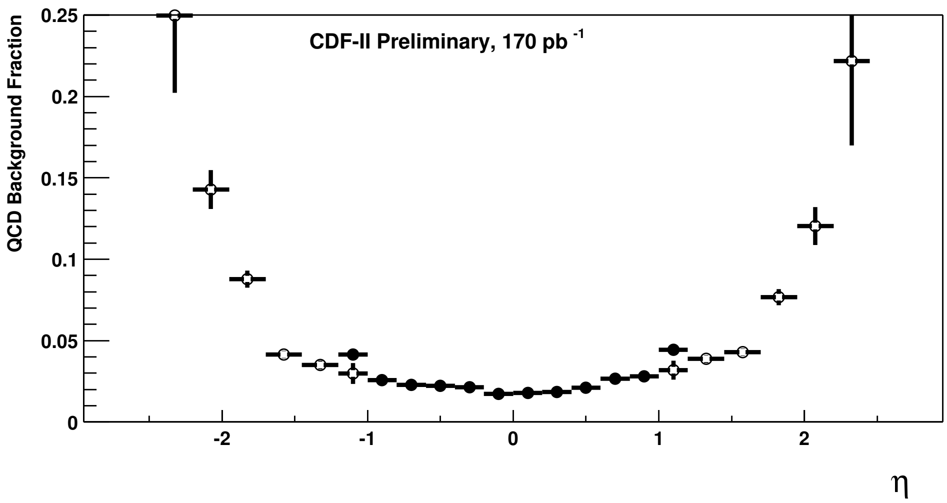

Figure 8: The measured QCD background fraction, F_{QCD}, as a function of eta. Open circles are from the plug triggers, filled circles are from the central triggers. As noted in the text, this is an upper limit on the QCD background because it does not include all the cuts.

$Z \rightarrow e^+e^-$ events in which one of the leptons is lost represent a small but asymmetric background. We determine this background with a sample of 700,000 events from the zewk1e MC sample. 31,000 events pass the selection, and the resulting electron and positron counts, multiplied by a scale factor

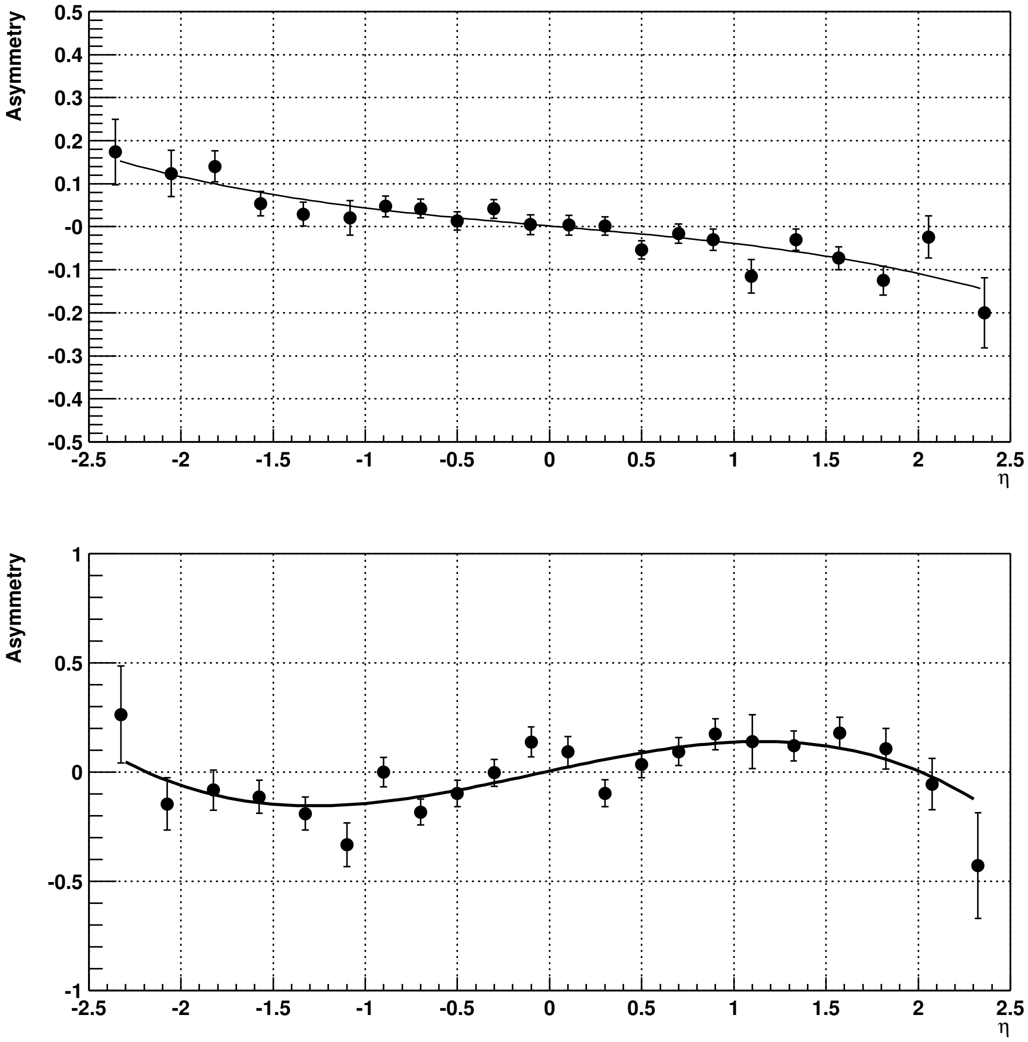

Figure 9: The asymmetry, $A(\eta)$, from MC for the $Z \rightarrow e^+e^-$ background (top) and the $W \rightarrow \tau\nu \rightarrow e\nu\nu$ background (bottom). The curves are from fits drawn simply to guide the eye.

of 0.028 ± 0.004 to account for the sample's luminosity, are subtracted bin by bin. The asymmetry of this background is shown in **Figure 9(a)**.

$W \to \tau\nu \to e\nu$ events bias the measured asymmetry because the τ decay dilutes the information available in the electron's direction. We determine this background with a sample of 675,000 events from the wewk1t MC sample. 5819 events pass the selection, and the resulting electron and positron counts, multiplied by a scale factor of 0.56 ± 0.08 to account for the sample's luminosity, are subtracted bin by bin. The asymmetry of this background is shown in **Figure 9(b)**.

The statistical uncertainty of the background corrections are folded into the systematic uncertainty on the asymmetry.

8 Results

Figure 10 shows the fully corrected asymmetry as a function of η and $|\eta|$.

Figure 11 compares the measured asymmetry, $A(\eta)$ to the prediction from PYTHIA with CTEQ5L.

9 E_T dependence

The measured asymmetry probes a large range of x for the initiating u and d quarks, from an upper value of approximately 5×10^{-1} where valence quarks dominate down to 2×10^{-3} where sea quarks dominate. The larger $|\eta|$ bins correspond, on average, to the extreme values of x. For example, a high x u quark and a low x $\bar{d}$ quark lead to W^+ with large p_Z and therefore large rapidity. The decay asymmetry dilutes this in the η of the $e^{\pm}$. Direct sensitivity to the PDFs, $u(x)$ and $d(x)$, would be improved by reducing this decay dilution. Ideally, reconstructing the W direction would remove it. As

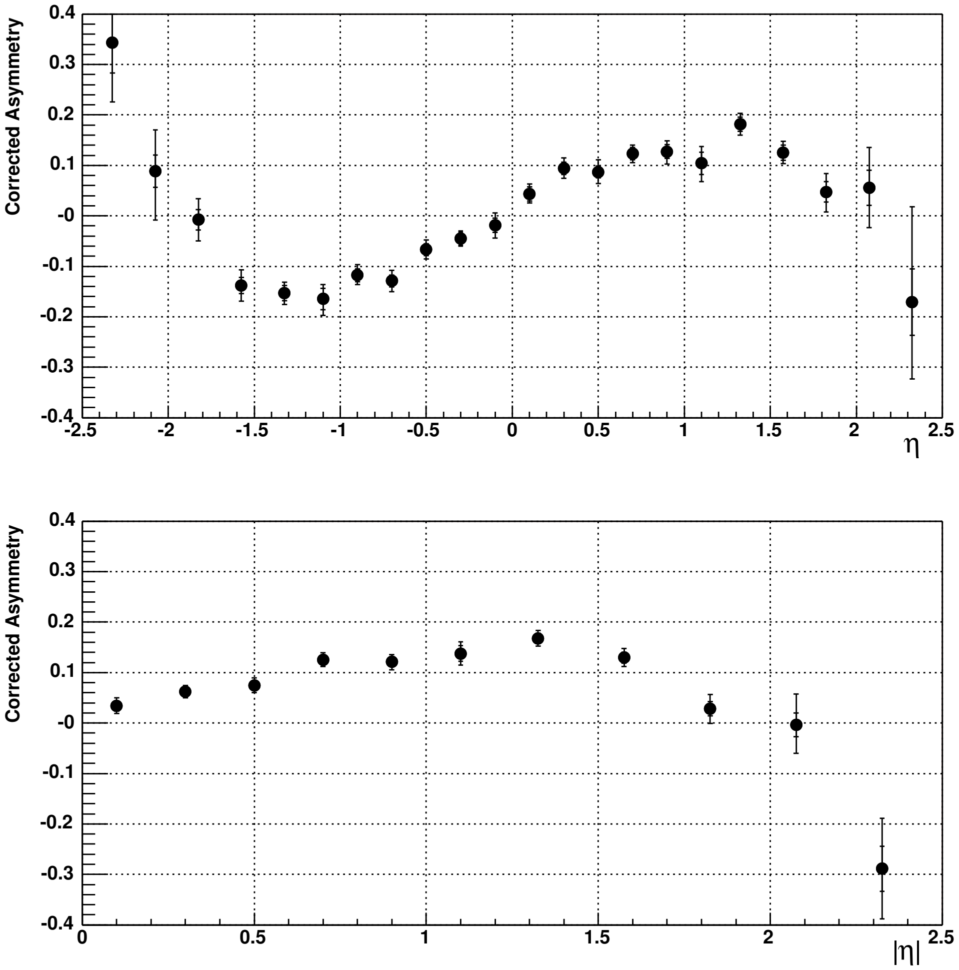

Figure 10: The fully corrected charge asymmetry is plotted as a function of η. The lower plot combines positive and negative η. Both statistical and total (statistical+systematic) uncertainties are shown.

described above, the unmeasured p_Z of the neutrino complicates this. However, we can improve the correspondence between η_e and y_W based on the kinematics of just the electron, which is well measured. The neutrino p_Z am-

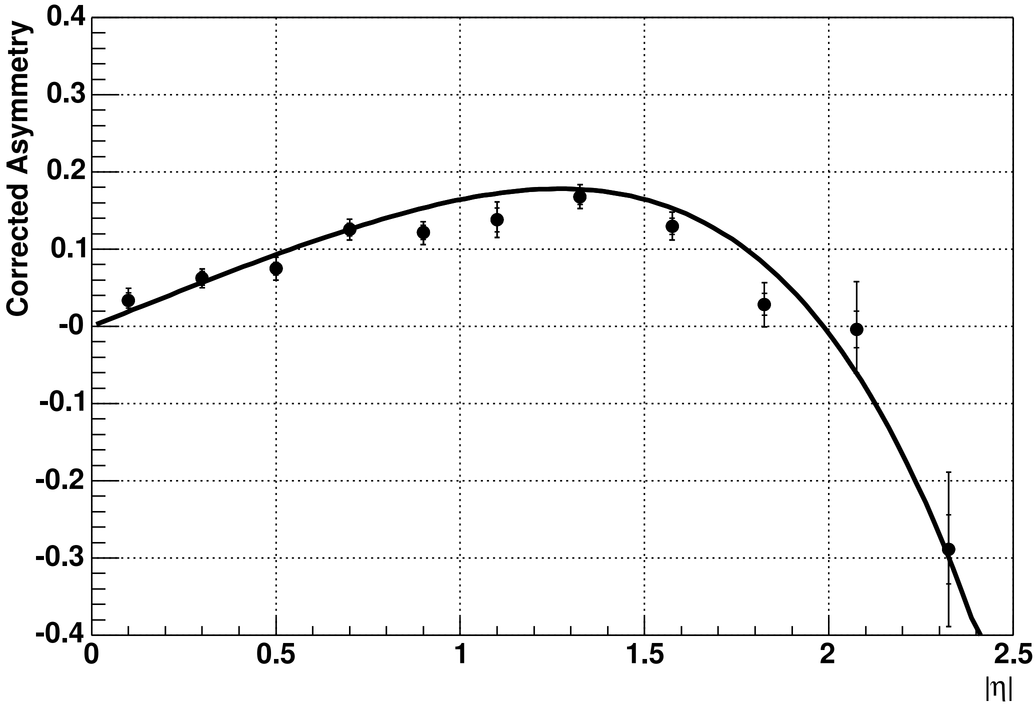

Figure 11: The measured asymmetry, $A(\eta)$, is compared to the prediction from PYTHIA with a CTEQ5L PDF.

biguity is a smaller effect for electrons near the Jacobian peak than for those at low E_T. We exploit this by separating the asymmetry measurement into bins of electron E_T. The size of the statistical and systematic uncertainties allow two bins, $25 < E_T < 35$ GeV and $35 < E_T < 45$ GeV. Events with even higher E_T are not useful because the QCD background dominates above the upper edge of the Jacobian peak.

The effect of this kinematic binning is illustrated in **Figure 12** which plots the W boson rapidity as determined with PYTHIA using the CTEQ5L PDF. The two E_T regions probe different W rapidities, and therefore different

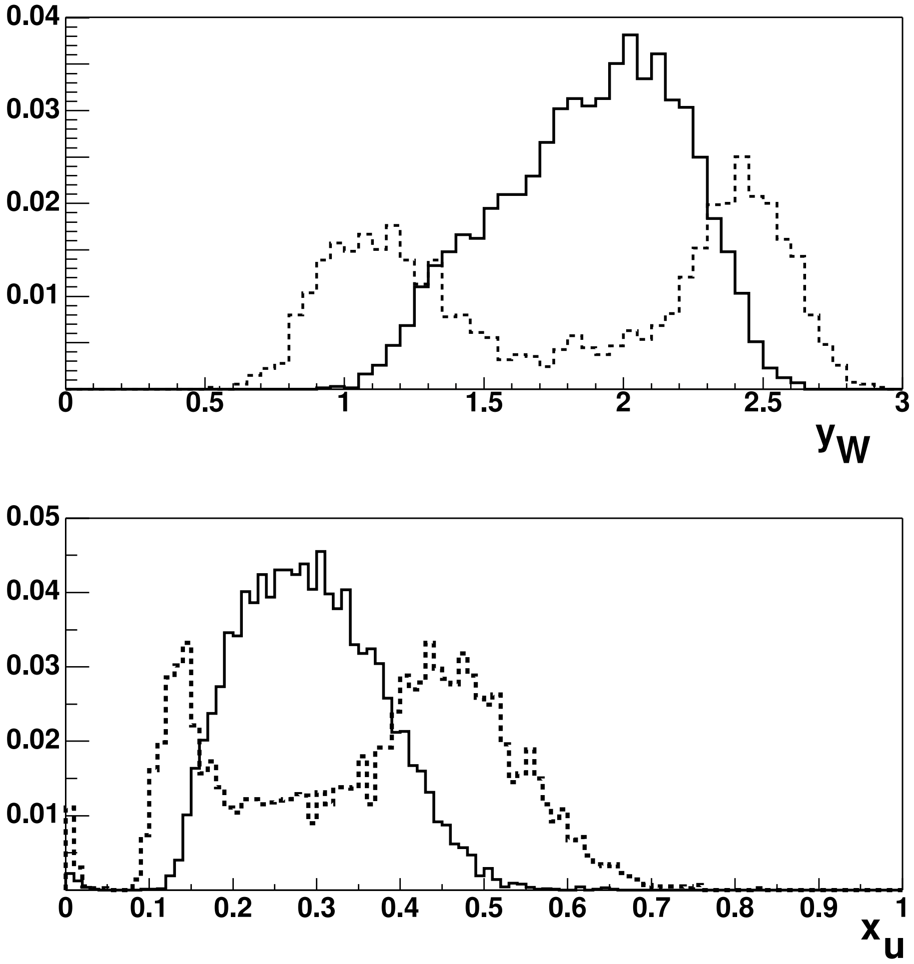

Figure 12: To illustrate the effect of the E_T binning, the distribution of W boson rapidity, y_W, and the u quark x are plotted for $W^+ \to e^+\nu$ events with positron $\eta \approx 1.8$. The distributions are normalized to unit area. The dashed curves are for positrons with $25 < E_T < 35$ GeV. The solid curves are for $35 < E_T < 45$ GeV. The two E_T regions probe different W rapidities and therefore different ranges of x, and the spread from the W decay distribution is reduced at higher E_T.

ranges of x. The decay distribution in the W rest frame causes a spread that is large for the low E_T bin and reduced in the higher E_T bin. Measuring the asymmetry separately in the two bins distinguishes this structure and allows a finer probe of the x dependence.

The asymmetry predicted by PYTHIA CTEQ5L for these two E_T ranges is illustrated in **Figure 13**.

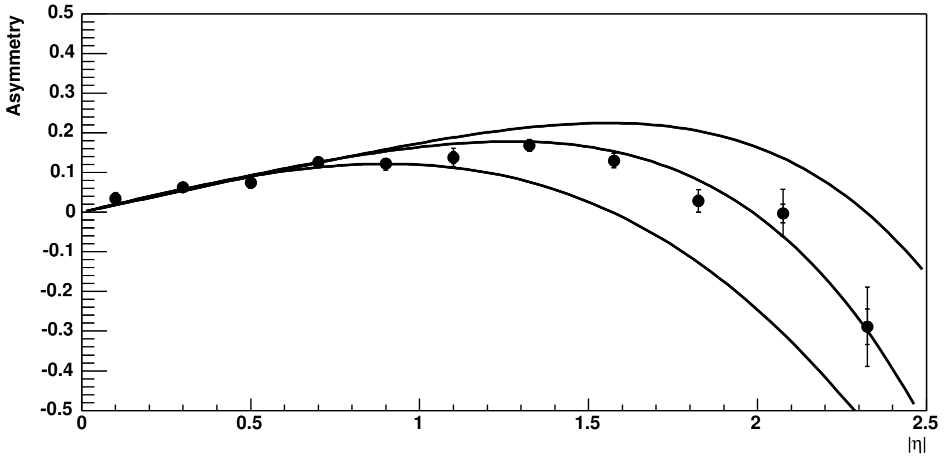

Figure 13: The effect of splitting the data into two E_T bins is illustrated by comparing the asymmetry predicted with PYTHIA CTEQ5L for three choices of E_T. The lower curve is $25 < E_T < 35$. The upper curve is $35 < E_T < 45$. The middle curve and points are $E_T > 25$.

The background and charge misidentification corrections are also E_T dependent, so we calculate and apply them separately for each E_T bin. The charge misidentification rate, f_Q, is compared as a function of η and E_T in **Figure 14**. The raw asymmetry is plotted for each of the E_T bins in **Figure 15**. The average charge mis-identification rate and the difference between the electron and positron mis-identification rates are plotted for each E_T bin in **Figure 16** and **Figure 17**, respectively.

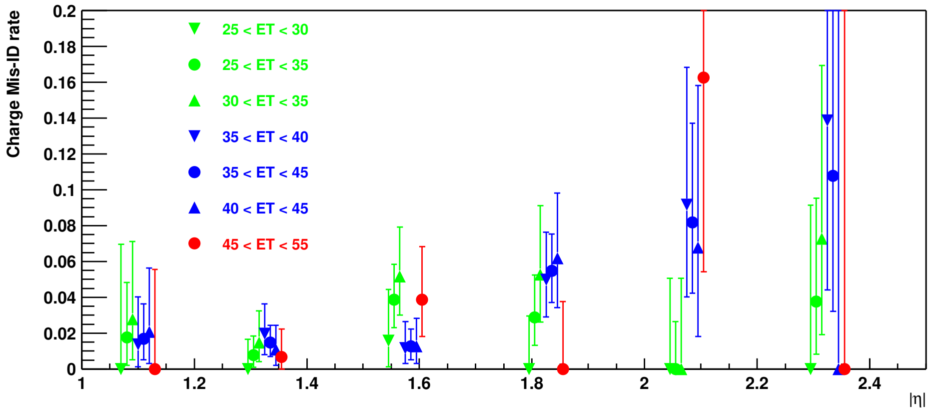

Figure 14: The charge misid rate, f_Q, as a function of η for various E_T ranges. There is some evidence of the expected increase in f_Q at higher E_T.

With the E_T dependent selection, and E_T dependent corrections, the measured asymmetry is compared to predictions from PYTHIA CTEQ5L in **Figure 18**. The CTEQ5L prediction is not well matched to the data particularly when separated by E_T.

10 PDF fits

In **Figure 18**, the PYTHIA CTEQ5L prediction does not describe the data very well when separated by E_T range. That is not surprising for two reasons. First, the PDFs are really only known from fits to previous data. The W asymmetry probes regions of x and Q^2 which are not well constrained by other low energy data. CTEQ5L *does* include fits to the Run 1 W asymmetry measurement, but that did not separate the data by E_T range. Second, the W p_T spectrum is likely to be poorly modelled by the LO PYTHIA. A better description is provided by NLO RESBOS Monte Carlo which incorporates

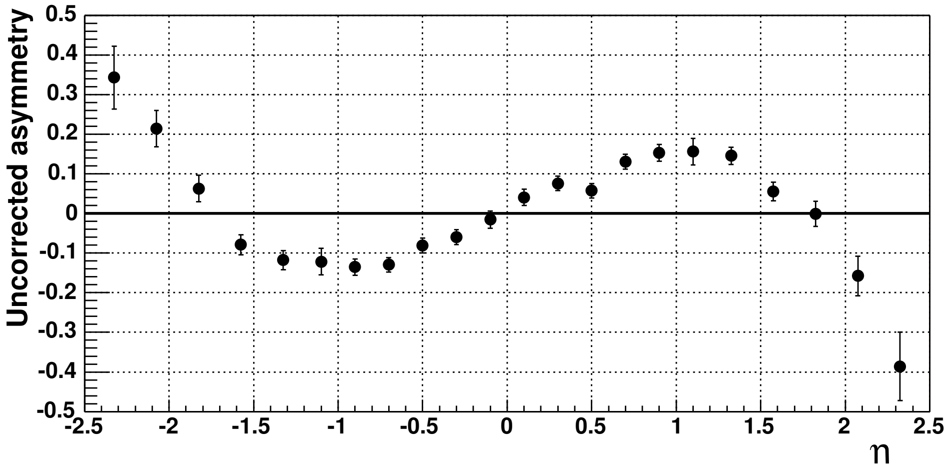

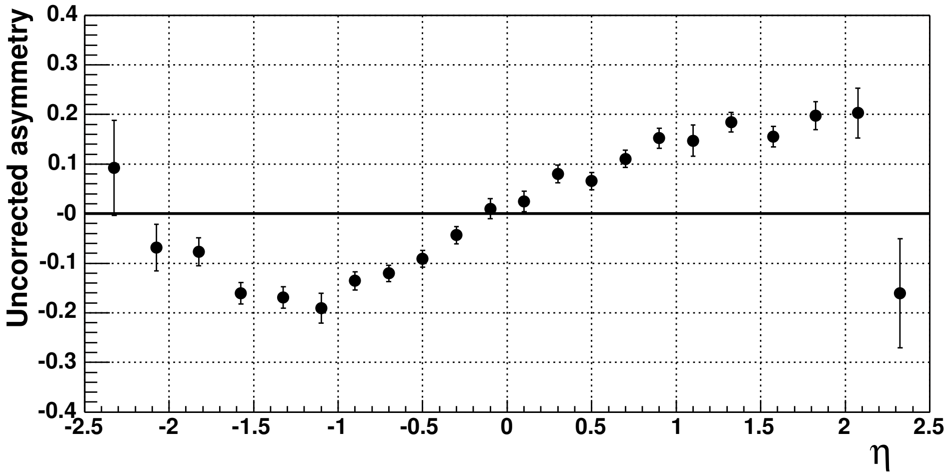

Figure 15: The raw asymmetry is plotted as a function of η for the two E_T bins. The top plot is $25 < E_T < 35$ GeV. The bottom plot is $35 < E_T < 45$ GeV.

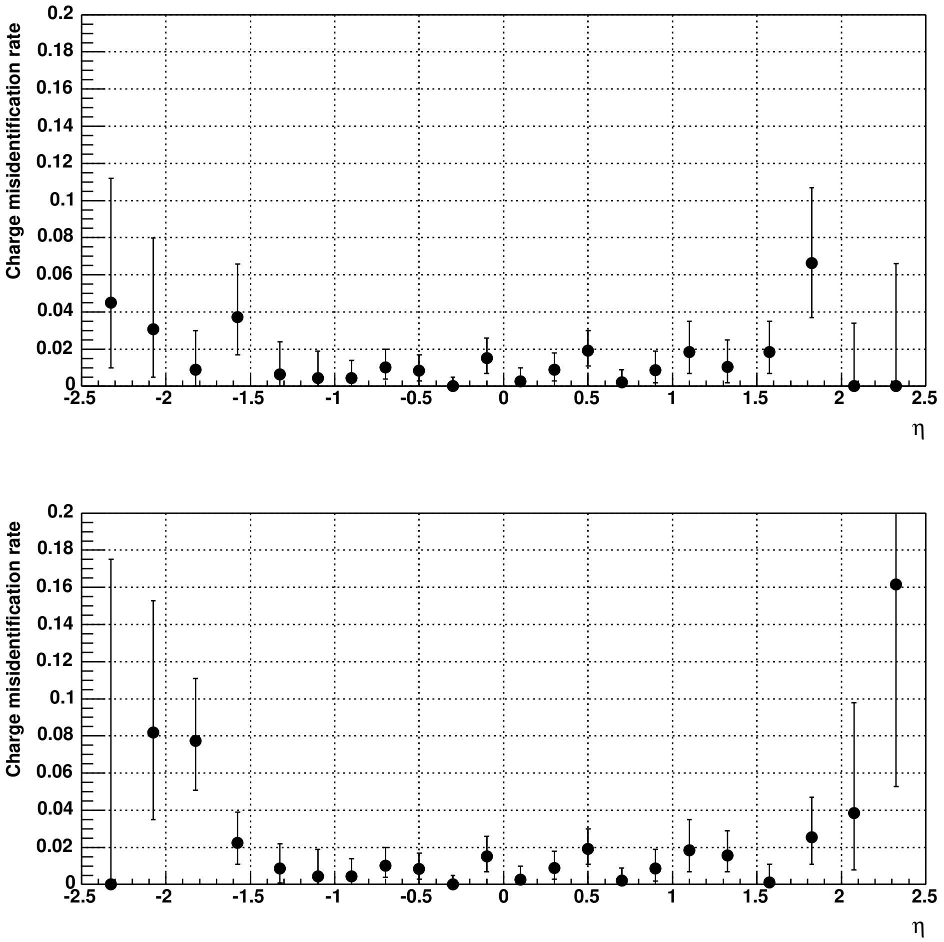

Figure 16: The charge mis-identification rate is plotted as a function of η for the two E_T bins. The top plot is $25 < E_T < 35$ GeV. The bottom plot is $35 < E_T < 45$ GeV.

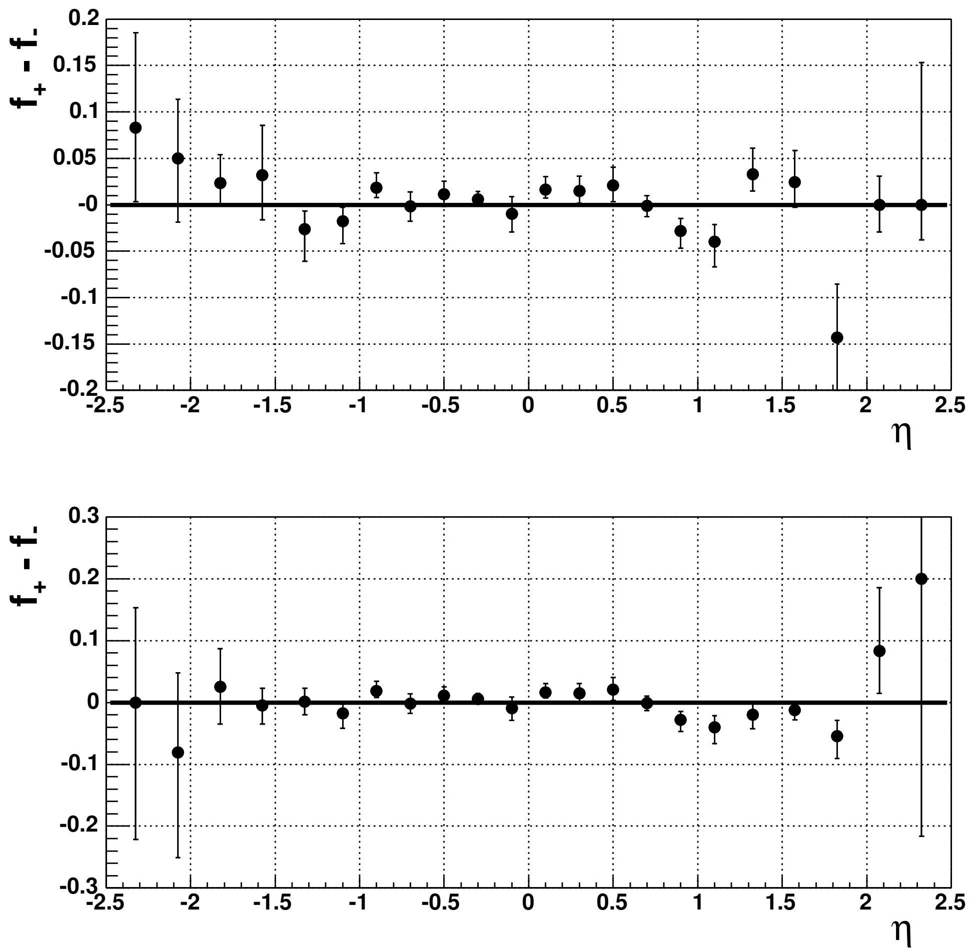

Figure 17: The charge dependent difference in mis-identification rate, $f_{+} - f_{-}$, is plotted as a function of η for the two E_T bins. The top plot is $25 < E_T < 35$ GeV. The bottom plot is $35 < E_T < 45$ GeV.

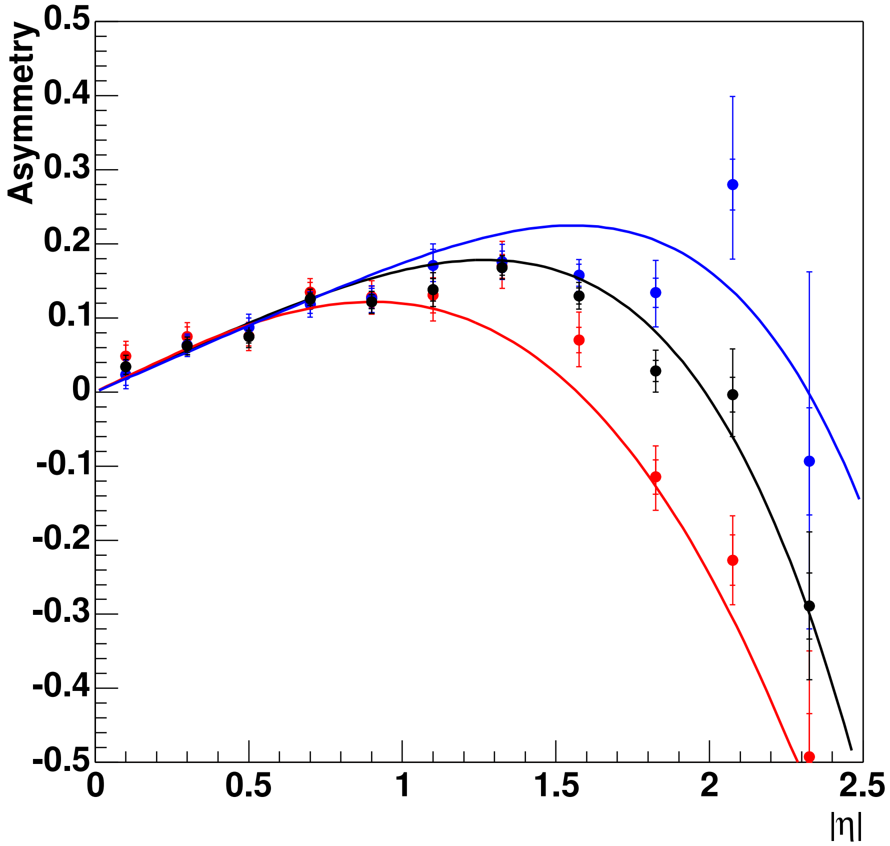

Figure 18: The PYTHIA CTEQ5L prediction is compared to the measured asymmetry for three choices of E_T. The lower, red, curve is $25 < E_T < 35$. The upper, blue, curve is $35 < E_T < 45$. The middle, black, curve is $E_T > 25$. The prediction is not well matched to the data in either E_T range.

soft gluon resummation [9]. However, RESBOS produces event weights and cannot be interfaced to cdfSim. It can only be compared at generator level.

The goal of the measurement is to provide data to be included in global PDF fits. Such fits cannot use cdfSim. They could parametrically model the detector effects such as resolution and efficiency, however we have studied these effects and found them to be negligible. (Indeed, the choice of separating the data into ranges of electron E_T, rather than missing E_T or transverse mass, is motivated by the precision with which that quantity is measured.) **Figure 19** demonstrates this by plotting the difference in asymmetry at simulated and generator level as a function of $|\eta|$. The differences are small compared to the uncertainty on the data, so comparison at generator level is appropriate for the fits. These generator-simulated differences are folded into the systematic uncertainties.

We compare the measured asymmetry to the CTEQ6.1M and MRST02 PDFs using NLO RESBOS for the two ranges of E_T in **Figure 20**. The predictions in the lower E_T region describes the data fairly well. In the high E_T region, both predictions are somewhat high indicating that $u(x)/d(x)$ needs to be decreased.

Inclusion of this data in updated fits is in progress, thanks to Joey Huston. To facilitate this, the results are tabulated in Table 1.

11 Cross checks

We have performed several cross-checks of the measurement.

We validate the calculation of the asymmetry and its statistical error by producing an artificial $A(\eta)$ and verifiying that it is properly measured with appropriate pulls.

In the central region, when we have a COT track, we compare the asymmetry measured with the COT track to what is measured using Phoenix tracks and find negligible difference.

By CP invariance, $A(\eta) = -A(-\eta)$. We check this in **Figure 21** by adding the west and east asymmetry for each bin of $|\eta|$. The results are consistent with zero with a χ^2 of 9.5 with 11 degrees of freedom.

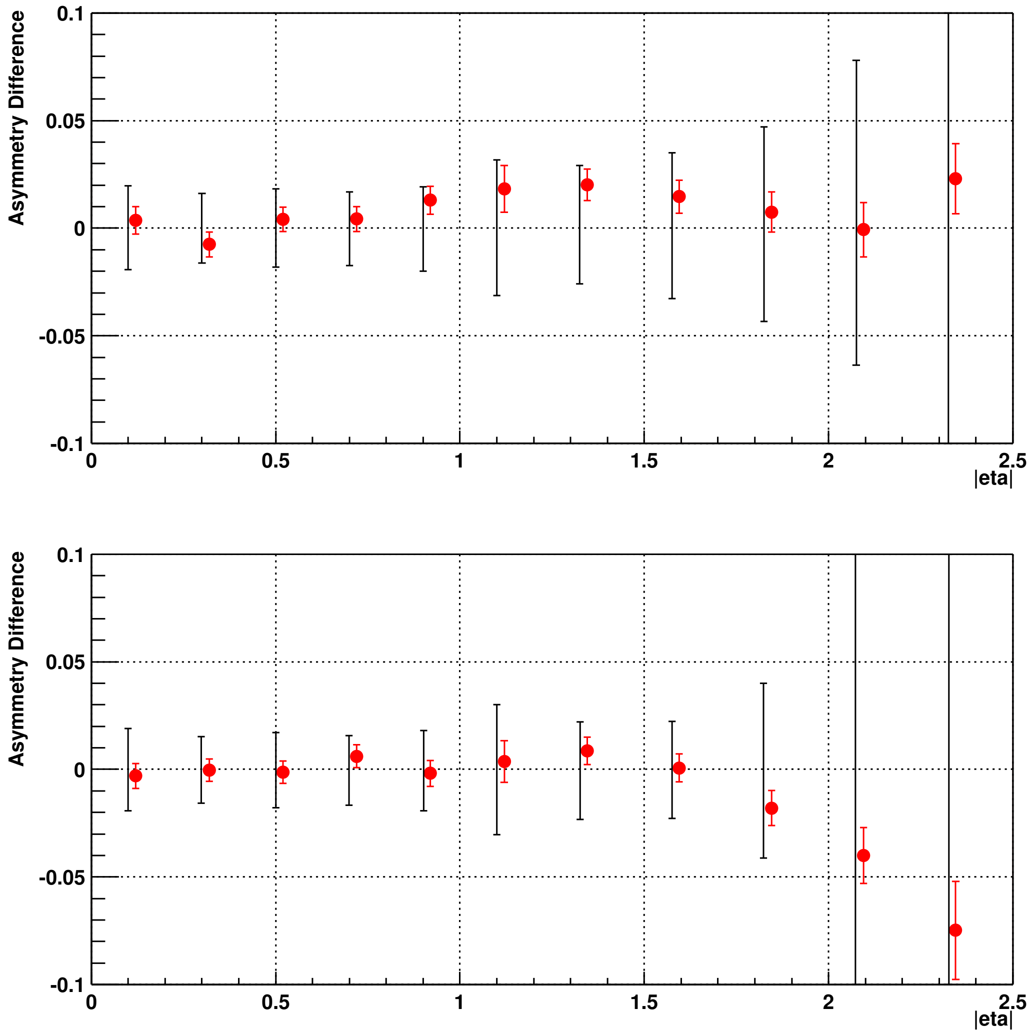

Figure 19: The red points show the difference between the asymmetry calculated after simulation from that obtained with the same kinematic cuts applied at generator level using PYTHIA CTEQ5L. The black bars indicate the uncertainty from the data in each $|\eta|$ bin. The upper plot is $25 < E_T < 35$. The lower plot is $35 < E_T < 45$. These asymmetry differences are folded into the systematic uncertainties.

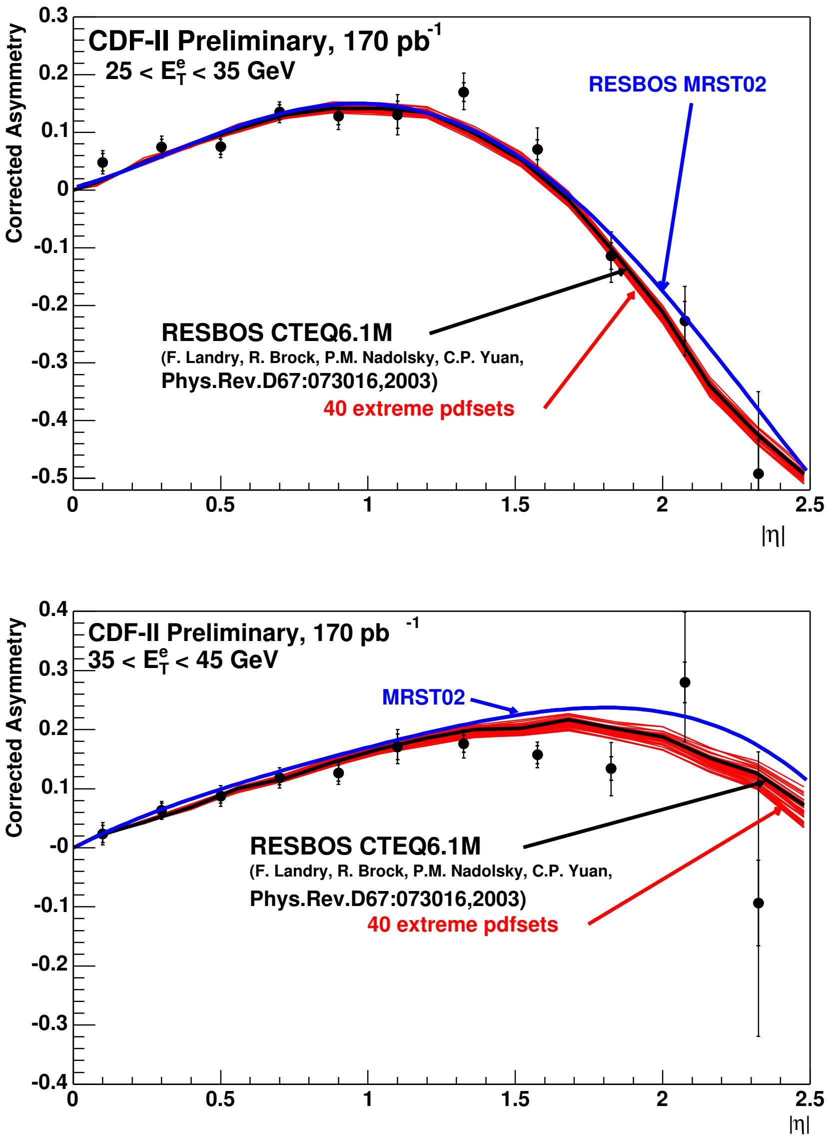

Figure 20: The measured asymmetry, $A(\eta)$, is compared to the expectation from the CTEQ6.1m and MRST02 PDFs in RESBOS for the two different ranges of electron E_T. The upper plot is for $25 < E_T < 35$ GeV. The lower plot is for $35 < E_T < 45$ GeV.

$\|\eta\|$	$A(\|\eta\|)$		
	$E_T > 25$	$25 < E_T < 35$	$35 < E_T < 45$
0.11	$3.4 \pm ^{1.6}_{1.5}$	4.8 ± 2.0	2.3 ± 1.9
0.30	6.2 ± 1.2	7.5 ± 1.9	6.3 ± 1.5
0.50	7.5 ± 1.5	7.5 ± 1.9	8.8 ± 1.8
0.70	12.6 ± 1.3	13.5 ± 1.8	11.8 ± 1.7
0.89	$12.2 \pm ^{1.6}_{1.4}$	12.8 ± 2.3	$12.6 \pm ^{1.7}_{1.9}$
1.09	13.8 ± 2.3	13.1 ± 3.5	17.1 ± 2.9
1.33	16.8 ± 1.6	$17.0 \pm ^{3.4}_{3.0}$	17.6 ± 2.4
1.57	13.0 ± 1.8	$7.0 \pm ^{3.8}_{3.6}$	15.7 ± 2.2
1.81	2.9 ± 2.9	$-11.5 \pm ^{4.2}_{4.5}$	$13.4 \pm ^{4.4}_{4.6}$
2.04	$-0.4 \pm ^{6.2}_{5.7}$	-23 ± 6	$28 \pm ^{12}_{10}$
2.31	-29 ± 10	-49 ± 14	$-9 \pm ^{26}_{23}$

Table 1: The measured asymmetry values are tabulated in percent. The listed $|\eta|$ is the event weighted average. Asymmetric uncertainties listed for some values arise because of the Poisson and binomial statistics inherent in the event counting.

Uncertainty on the plug alignment constants, particularly $\Delta\phi$, can bias the charge identification and thus the asymmetry measurement. Any such residual misalignments should be accounted for in the uncertainty on the charge misidentification rate measured from Z data. We check this by moving the alignment constants by about twice their uncertainty and verifying that the results change by less than the systematic uncertainty.

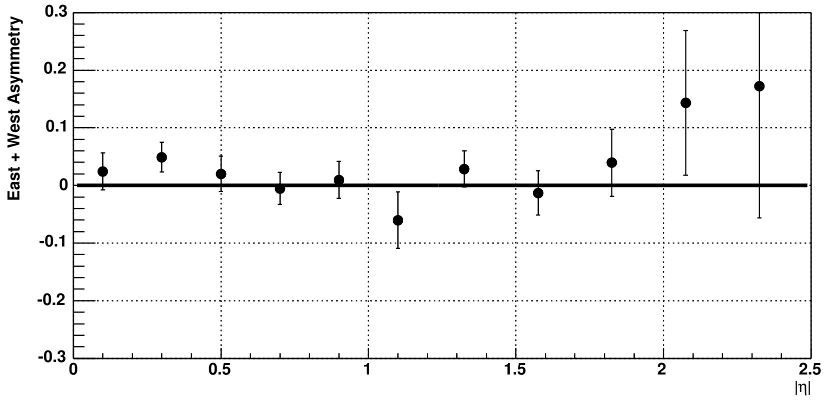

Figure 21: To check that the asymmetry measured at η is the negative of the asymmetry at $-\eta$, as expected, the sum of $A(\eta)$ and $A(-\eta)$ is plotted as a function of $|\eta|$. The χ^2 probability relative to zero is about 60%, so we see no significant evidence of an east-west asymmetry in the asymmetry.

12 Conclusions

We have measured the W charge asymmetry in the $e\nu$ channel. The results will improve PDF fits, particularly at high $|\eta|$ and high E_T.

References

[1] F. Abe *et al.* (CDF Collaboration), Phys. Rev. Lett. **81**, 5744 (1998)

[2] J. Goldstein, C. Issever, T. Nelson, R. Snider, D. Stuart, *Silicon Tracking for Plug Electrons*, CDF Note 5970

[3] http://www-cdf.fnal.gov/internal/dqm/goodrun/v4/goodv4.html

[4] C. Issever, D. Stuart, R. Taylor *Plug Alignment*, CDF Note 6108

[5] L. Lyons, private communication

[6] Roger Barlow, http://www.slac.stanford.edu/econf/C030908/papers/WEMT002.pdf

[7] C. Issever, A. Scott, D. Stuart *QCD Backgrounds for W's in the plug*, CDF Note 6412

[8] J. Conway, *Efficiency Uncertainties: A Bayesian Prescription*, CDF Note 5894

[9] F. Landry, R. Brock, P. M. Nadolsky, C. P. Yuan, Phys. Rev. D **67**, 073016 (2003).